Supporting Information

Culik et al. 10.1073/pnas.1721022115

SI Text

As described in the main text, Zn^{2+} was added progressively to a solution of apoSOD1^{2SH} and the intensities of the cross-peaks in ^{1}H–^{15}N correlation spectra were quantified as a function of added metal (Fig. 2). The intensity profiles of the residues were fit to a sequential binding model of the form:

$$A + B \overset{K_1}{\rightleftharpoons} AB$$

$$AB + B \overset{K_2}{\rightleftharpoons} AB_2, \qquad \text{[S1]}$$

where A refers to apoSOD1^{2SH} and B to Zn^{2+}. The dissociation constants for Zn^{2+} binding to the Zn (K_{d1}) and the Cu (K_{d2}) sites are inverses of K_1 and K_2, respectively, such that

$$K_1 = \frac{1}{K_{d1}} = \frac{[AB]}{[A][B]} \qquad \text{[S2]}$$

and

$$K_2 = \frac{1}{K_{d2}} = \frac{[AB_2]}{[AB][B]}. \qquad \text{[S3]}$$

If A_T and B_T are the total concentrations of protein (SOD1^{2SH}) and Zn^{2+} in solution at any titration point, the mass balance equations for this system can be written as follows:

$$A_T = [A] + [AB] + [AB_2] \qquad \text{[S4]}$$

and

$$B_T = [B] + [AB] + 2[AB_2], \qquad \text{[S5]}$$

which gives

$$[A] = A_T - [AB] - [AB_2] \qquad \text{[S6]}$$

and

$$[B] = B_T - [AB] - 2[AB_2]. \qquad \text{[S7]}$$

Inserting Eq. **S7** into Eq. **S3** and solving for $[AB_2]$ gives the following:

$$[AB_2] = \frac{[AB](B_T - [AB])}{K_{d2} + 2[AB]}. \qquad \text{[S8]}$$

Substituting for $[A]$ and $[B]$ in Eq. **S2** using Eqs. **S6** and **S7**, and further replacing $[AB_2]$ in terms of $[AB]$ from Eq. **S8**, yields a cubic equation in $[AB]$:

$$a[AB]^3 + b[AB]^2 + c[AB] + d = 0, \qquad \text{[S9]}$$

where

$$a = 4K_{d1} - K_{d2},$$
$$b = 4K_{d1}K_{d2} - K_{d2}^2 + 2K_{d2}A_T,$$
$$c = K_{d1}K_{d2}^2 + K_{d2}^2A_T + K_{d2}^2B_T + K_{d2}B_T^2 - 2K_{d2}A_TB_T,$$
$$d = -K_{d2}^2A_TB_T.$$

The concentration of $[AB]$ at every point in the titration corresponding to specific A_T and B_T values was calculated by numerically solving for the roots of Eq. **S9**. The correct root was identified through a two-level selection process where roots were discarded if they were negative or larger than A_T. $[AB_2]$ was determined from $[AB]$ using Eq. **S8**, while $[B]$ was subsequently obtained from $[AB]$ and $[AB_2]$ (Eq. **S5**). Concentrations were then converted to intensities in the fitting routine using relations provided in Fig. 2, which are specific for each class of peak (see text).

SI Materials and Methods

NMR Spectroscopy. All NMR spectra were acquired on a Varian 600 MHz (14.1 T) spectrometer equipped with a cryogenically cooled probe. The sample temperature was measured using a thermocouple placed inside an NMR tube; all experiments were performed at 25 °C.

CEST. All ^{15}N-CEST datasets were acquired at 600 MHz using a previously reported pulse sequence (52), an exchange duration, T_{relax}, of 350 ms, and weak B_1 fields ranging between 21.5 and 26.5 Hz (depending on the experiment), calibrated as described earlier (52). Pseudo-3D datasets containing 89 planes were collected, corresponding to a total acquisition time of 50 h, with the position of the weak B_1 field ranging between 94 and 137 ppm.

CPMG. ^{15}N-CPMG datasets were acquired at a static magnetic field of 600 MHz (14.1 T) using a previously reported pulse scheme (53) and a constant-time CPMG element of 30 ms. Each pseudo-3D experiment comprised 22 ν_{CPMG} values, ranging from 33.3 to 1,000 Hz, with three points repeated for error analysis (54), giving rise to net acquisition times of ∼17 h per experiment.

Data Analysis. NMR datasets were processed with nmrPipe (55) and visualized using nmrDraw and Sparky (55, 56). Resonance intensities were quantified as a function of the frequency of the weak B_1 field in CEST experiments or the frequency of application of 180° pulses in CPMG experiments using the program FuDA (www.ucl.ac.uk/hansen-lab/), whereby peak line shapes were fit globally across all frequency values. CEST profiles, I/I_0 vs. B_1 field position, were constructed from peak intensities recorded with (I) and without (I_0) the relaxation interval, T_{relax}. CPMG profiles, $R_{2,eff} = -1/T_{relax}\ln(I/I_0)$ vs. ν_{CPMG}, were generated from measured I and I_0 values corresponding to peak intensities with (I) and without (I_0) the CPMG relaxation element of duration T_{relax} (24).

Backbone Assignment. Experiments for resonance assignments were recorded at 600 MHz using U-[^{13}C,^{15}N] pWT apoSOD1^{S-S}, pWT E,Zn-SOD1^{2SH}, and A4V E,Zn-SOD1^{2SH} samples. Assignments of backbone resonances were obtained using a combination of 2D ^{1}H–^{15}N HSQC and 3D HNCACB, CBCA(CO)NH, HNCO, and HN(CA)CO experiments (57), described in detail previously (58).

^{15}N R_1, $R_{1\rho}$, and $^{15}N\{^1H\}$ NOE Values. ^{15}N R_1 and $R_{1\rho}$ spin relaxation rates and $^{15}N\{^1H\}$ NOE values were measured using pulse sequences described previously (59–61). R_1 measurements were obtained with 10 relaxation delays from 10 ms to 1 s, while $R_{1\rho}$ experiments were based on eight relaxation delays varying from 2 to 50 ms. Residue-specific R_1 and $R_{1\rho}$ values were obtained from fits of peak intensities vs. relaxation time to a single exponential decay function, while NOE ratios were ascertained directly from intensities in experiments recorded with (5-s relaxation delay followed by 7-s saturation) and without (relaxation delay of 12 s) ^{1}H saturation. Errors in NOE values were calculated

by propagating the error in the respective peak intensities. $R_{1\rho}$ values were converted to R_2 rates using the standard relation, $R_{1\rho} = R_2\sin^2\theta + R_1\cos^2\theta$, where $\theta = \tan^{-1}(B_{SL}/\delta)$, B_{SL} is the spin-lock field strength (~2 kHz), δ is the resonance offset of the spin in question (in hertz), and θ is the angle of the effective field and the z axis.

Isothermal Titration Calorimetry. Samples of E,Zn-SOD1^{2SH} for isothermal titration calorimetry (ITC) were prepared by adding a stoichiometric amount of $ZnSO_4$ to apoSOD1^{2SH} (0.7–2 mM total monomer) followed by sample incubation at room temperature under anaerobic conditions for 30 min. ITC experiments were performed as described previously (29), using a Microcal Isothermal Titration Calorimetry 200 instrument (Malvern). Small volumes (0.4–0.5 μL) of concentrated pWT E,ZnSOD1^{2SH} solution were injected into an identical buffer in the ITC reaction cell.

SOD1/CCS Chromatography-Based Binding Assays. Proteins (purified SOD1 of the appropriate maturation state, CCS, or purified SOD1+CCS) were injected (total volume of 200 μL using 50 μM protein concentrations) onto a HiLoad 16/60 Superdex 75 column (GE Healthcare) with a 1-mL sample loop, 0.5 mL/min flow rate, and buffer composition of 20 mM MES, 1 mM TCEP, pH 6.3. For runs combining SOD1 with CCS, samples were mixed together at room temperature and incubated for 30 min before injection.

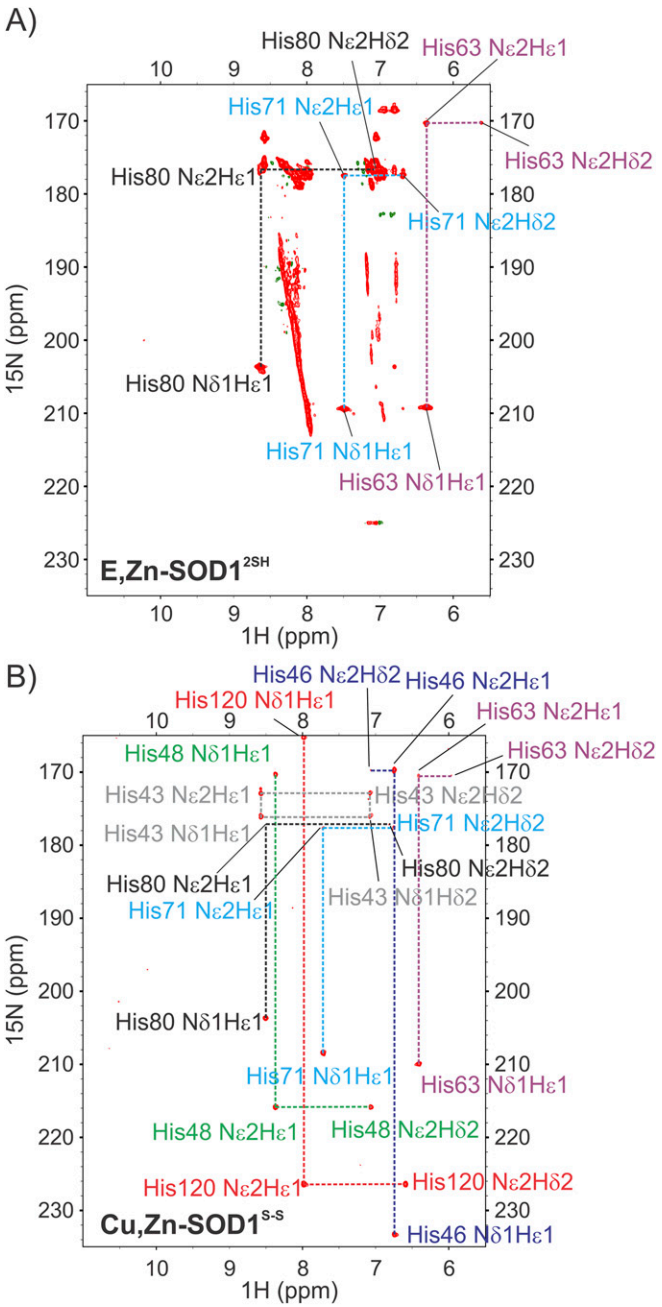

Fig. S1. Zn initially binds the SOD1 Zn site. (*A*) Side-chain ^{1}H–^{15}N HMBC spectrum of E,Zn-SOD1^{2SH} with the residue-specific cross-peaks of His side chains connected with colored lines (black for H80, cyan for H71, and purple for H63). All three His ligands of the Zn ion, 63, 71, and 80, resonate at chemical shifts identical to those observed in Cu,Zn-SOD1$^{S\text{-}S}$ (*B*) demonstrating that the first Zn binding site in apoSOD1^{SH} corresponds to the canonical Zn site. Note that the patterns of shifts indicate that the ligation of metal in the Zn site involves Nδ1 for all three His residues.

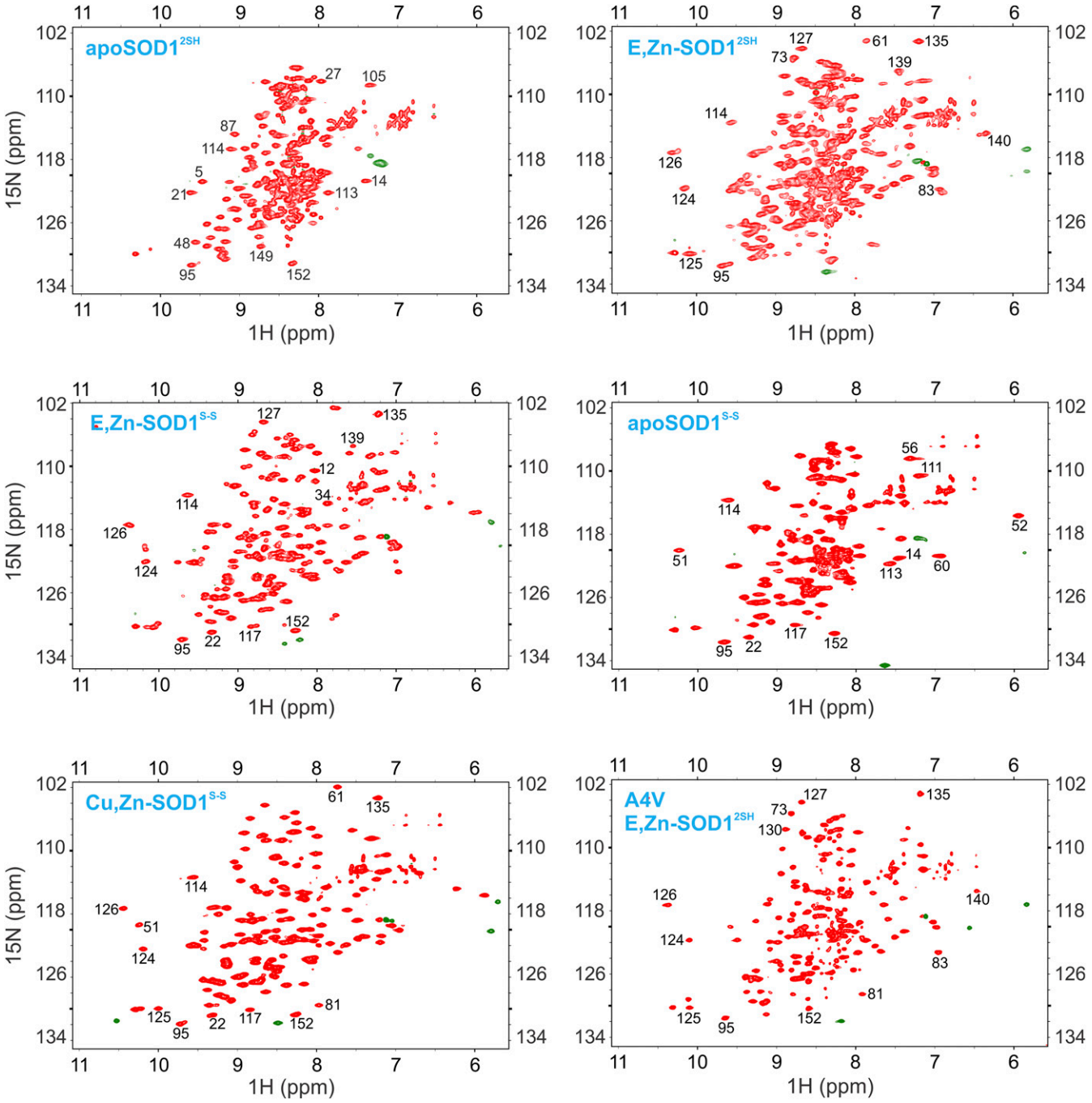

Fig. S2. $^{1}H–^{15}N$ HSQC spectra of SOD1 maturation intermediates. Representative spectra for SOD1 samples used in this study, as indicated (600 MHz, 25 °C). A number of peak assignments have been included; cross-peaks in green are aliased.

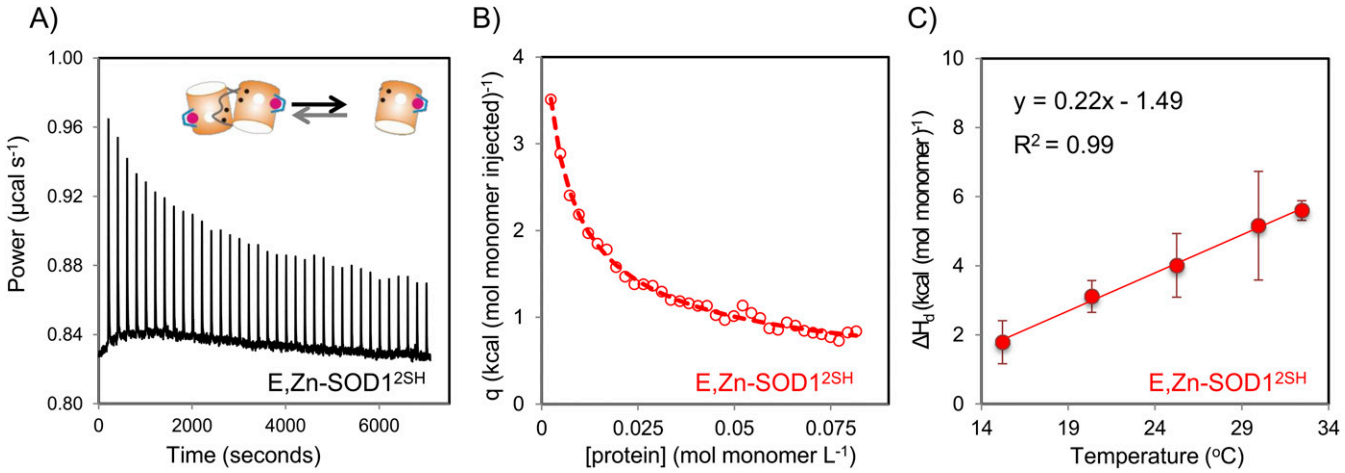

Fig. S3. ITC analysis of E,Zn-SOD1^{2SH} dimer dissociation. (*A*) Raw ITC data of dimer dissociation at 25 °C. Each peak corresponds to the heat measured for a small volume injection of protein solution into the ITC sample cell, which results in dimer dissociation, represented by the *Inset* schematic. The endothermic heats decrease with successive injections due to the increase in protein concentration in the cell. (*B*) The values of the integrated heat for each injection (*q*, circles) are fit to a dimer dissociation model (dashed line). (*C*) Kirchoff plot of ΔH_d vs. temperature. The ΔC_p, determined from the slope, is 0.22 ± 0.01 kcal·(mol monomer)$^{-1}$·°C^{-1}. Errors bars are the SDs for multiple experiments.

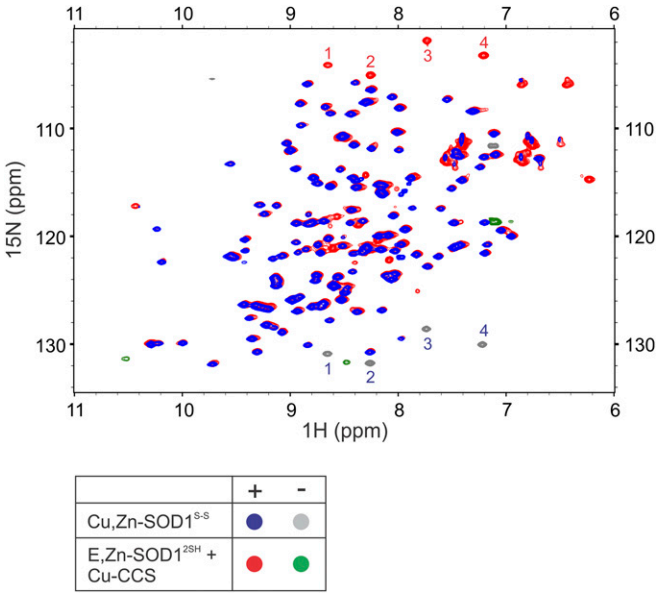

Fig. S4. E,Zn-SOD1^{2SH} matures to enzymatically active Cu,Zn-SOD1^{S-S} upon addition of Cu-loaded CCS. ^{1}H–^{15}N HSQC spectrum of Cu,Zn-SOD1^{S-S} (blue/gray) overlays well with a spectrum of a sample containing 1:2 E,Zn-SOD1^{2SH}:Cu/CCS (red/green) with both concentrations reported as monomers. Note that the gray and green cross-peaks are aliased and appear with negative intensity, as indicated in the legend. Peaks labeled as 1, 2, 3, and 4 in the Cu,Zn-SOD1^{S-S} spectrum (gray) match those in the spectrum of 1:2 E,Zn-SOD1^{2SH}:Cu/CCS with the same labels (red) that are not aliased.

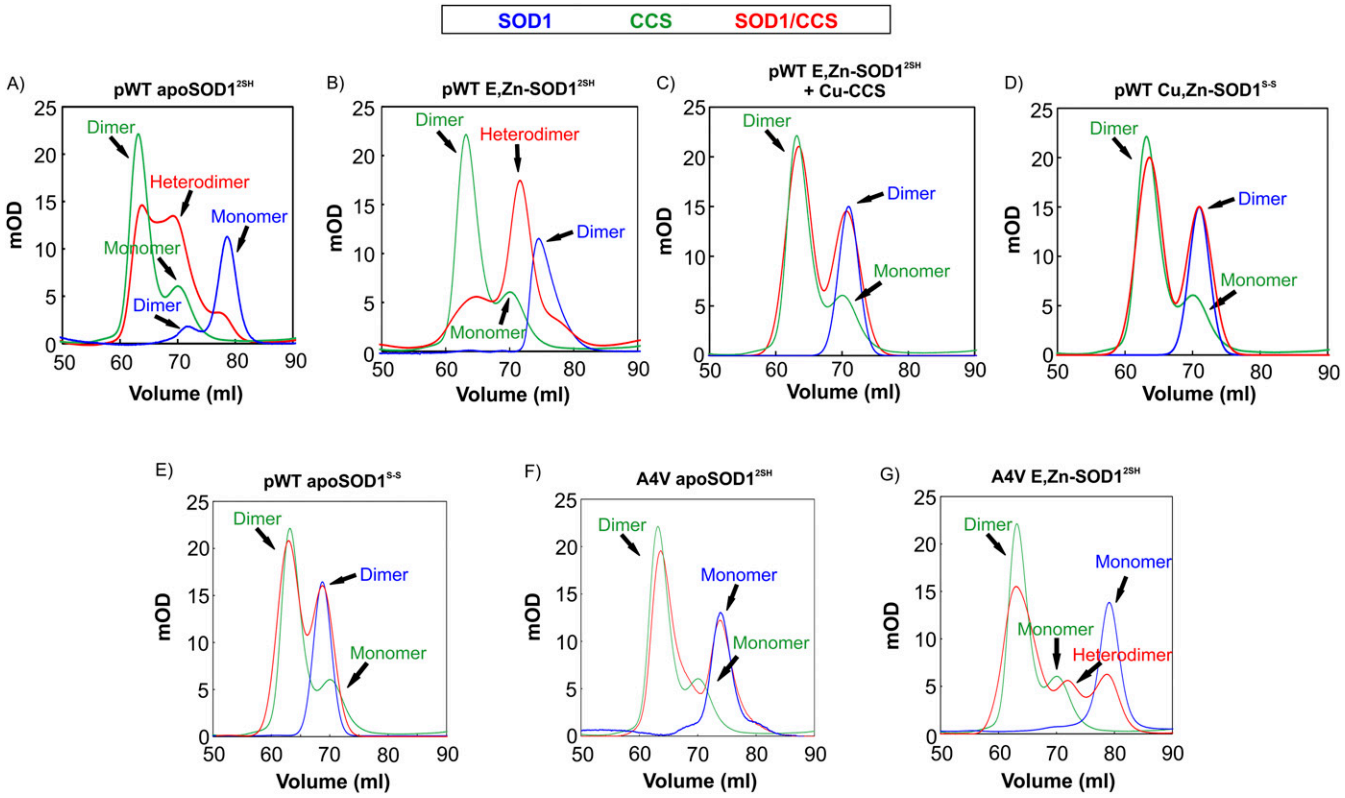

Fig. S5. Monomeric SOD1 is required for binding to CCS, and the presence of zinc increases formation of the heterodimer. (*A*–*G*) FPLC chromatogram traces of SOD1, CCS, or a 1:1 stoichiometric ratio of CCS and SOD1, as indicated, for the maturation states of pWT SOD1 highlighted in Fig. 1. The origin of each of the peaks is as labeled, with major peaks confirmed by native gel electrophoresis. Notably, a larger proportion of apoSOD1^{2SH} is able to bind to CCS upon addition of Zn^{2+} despite the largely dimeric nature of the Zn-protein (compare *A* and *B*). A similar scenario occurs for the A4V mutant except that addition of Zn^{2+} does not promote formation of heterodimer to the same extent as for pWT, showing that metallation does not completely "rescue" the A4V mutant. The traces for E,Zn-SOD1^{S-S} are identical to those for apoSOD1^{S-S} and are not shown. In each of the panels, with the exception of *C*, the blue trace corresponds to the maturation state of SOD1 indicated immediately above the panel. In contrast, in *C*, the SOD1 trace (blue) was measured for the Cu,Zn-SOD1^{S-S} state for comparison. The *y*-axis label refers to milli-optical density units.

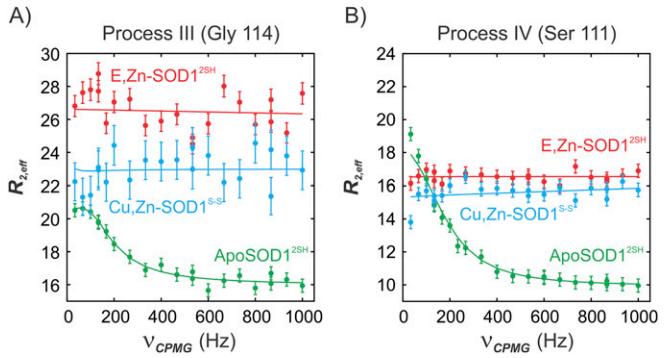

Fig. S6. Exchange processes III and IV have been quenched in E,Zn-SOD1^{2SH} and Cu,Zn-SOD1^{S-S}. CPMG profiles for Gly-114 reporting on process III (*A*) and Ser-111 reporting on process IV (*B*) for E,Zn-SOD1^{2SH} (red) and Cu,Zn-SOD1^{S-S} (cyan), compared with apoSOD1^{2SH} (green).